# Simulation of the Intraseasonal Oscillation in the ECHAM-4 Model: The Impact of Coupling with an Ocean Model*

SUSAN KEMBALL-COOK, BIN WANG,+ AND XIOUHUA FU+

*Department of Meteorology, School of Ocean and Earth Science and Technology, University of Hawaii at Manoa, Honolulu, Hawaii*

(Manuscript received 30 April 2001, in final form 4 September 2001)

ABSTRACT

Three 15-yr integrations were made with the ECHAM-4 atmospheric GCM (AGCM); in the first integration, the model lower boundary conditions were the observed monthly mean sea surface temperatures, and, in the second, the AGCM was coupled to the University of Hawaii 2.5-layer intermediate ocean model. In the third simulation, the SST climatology generated in the coupled run was used to create monthly mean SSTs, which were then used to drive the AGCM in an uncoupled configuration similar to the first run. The simulation of the intraseasonal oscillation (ISO) in these three runs was compared with data from the NCEP reanalysis and outgoing longwave radiation from NOAA polar-orbiting satellites, with particular emphasis on the boreal summer ISO.

The overall effect of coupling the AGCM to the ocean model is to improve the intraseasonal variability of the model. Upon coupling, the simulated boreal winter ISO becomes more spatially coherent and has a more realistic phase speed. In the May–June Asian monsoon season, the coupled run shows pronounced northward propagation of convection and circulation anomalies over the Indian Ocean, as in the observations, while northward propagation is absent in the uncoupled run. These improvements in the simulated ISO occur despite the fact that the coupled-run SST climatology has a substantial cold bias in both the Indian Ocean and the western Pacific warm pool. The improvement in the model ISO may be attributed to air–sea interaction whose mechanism is increased low-level convergence into the positive SST anomaly ahead of the convection anomaly.

The simulation of the August–October ISO is degraded upon coupling, however. The coupled-run basic state fails to produce the region of easterly vertical shear of the mean zonal wind, which lies on the equator during August–October. This region of easterly shear is critical for the emission of Rossby waves by equatorial convection associated with the ISO. In the absence of easterly shear, the observed northwestward propagation of convection is inhibited in both runs made using the coupled model basic state. The uncoupled AGCM run correctly locates the region of easterly shear and produces an August–October ISO that agrees well with observations.

## 1. Introduction

The intraseasonal oscillation (ISO) makes up a large fraction of the observed tropical intraseasonal variability. The ISO is a large-scale, generally eastward-propagating disturbance in the tropical circulation and convection with a period of approximately 30–60 days (Madden and Julian 1994). Recent observational and modeling studies have suggested that interactions between the ocean and the atmosphere occur on intraseasonal timescales and, further, that these interactions may be critical for the existence of the ISO. Understanding the role of coupling of the atmosphere and ocean is necessary for the prediction of the ISO, because air–sea interaction has been suggested to alter the structure, period, and coherence of the oscillation (e.g., Flatau et al. 1997; Waliser et al. 1999). In addition, for the purpose of modeling the global circulation, it is important to know whether a coupled GCM is required in order to correctly simulate the tropical intraseasonal variability.

Since Krishnamurti et al. (1988) first documented tropical air–sea interaction at intraseasonal timescales, a multitude of observational studies of air–sea interaction in the ISO have been performed. Many of these came out of Tropical Ocean Global Atmosphere Comprehensive Ocean–Atmosphere Response Experiment (TOGA COARE) and documented in detail the three ISO events that took place during the Intensive Observing Period (Gutzler et al. 1994; Weller and Anderson 1996; Lau and Sui 1997). Others have used Thermal Array in the Ocean buoy array data (Zhang 1996; Zhang

* School of Ocean and Earth Science and Technology Publication Number 5962 and International Pacific Research Center Publication Number 146.

+ Additional affiliation: International Pacific Research Center, University of Hawaii at Manoa, Honolulu, Hawaii.

*Corresponding author address:* Dr. Susan Kemball-Cook, Mail Stop 90-1116, Lawrence Berkeley National Laboratory, 1 Cyclotron Rd., Berkeley, CA 94720.
E-mail: srkemball-cook@lbl.gov

and McFadden 2000) and gridded datasets (Hendon and Glick 1997; Jones et al. 1998; Shinoda et al. 1998; Woolnough et al. 2000) to form composites of the ISO in order to examine the nature of the air–sea interaction.

Though most of the observational work on air–sea interaction in the ISO has focused on the winter Madden–Julian oscillation (MJO) mode, there have been several studies documenting interaction between ocean and atmosphere during the boreal summer ISO (BSISO). Krishnamurti et al. (1988), Lawrence and Webster (2001), and Kemball-Cook and Wang (2001) documented SST fluctuations that were coherent with ISO convective anomalies and showed northward propagation over the Indian Ocean. Kemball-Cook and Wang (2001) noted the presence of SST anomalies associated with the northwestward propagation of circulation and convection anomalies in the western Pacific during the August–October season. What is not clear from these observational studies of the ISO is whether the air–sea interaction is fundamental to the existence of the ISO, is merely a by-product of it, or plays a supporting role, such as intensification and organization of the disturbance. Several modeling studies have addressed this question.

Flatau et al. (1997) used observations from TOGA COARE to formulate an empirical relationship between wind speed and SST change on the equator. This relationship was then used in a highly idealized GCM to examine the effect of the SST feedback to the atmosphere on the behavior of equatorial convection. The SST feedback caused fluctuations in equatorial convection to become more organized and to have a slower eastward phase speed and a more realistic 50–60-day spectral peak in precipitation. This study, then, suggested that the simulation of the ISO was improved by the addition of a one-way feedback from the ocean to the atmosphere. Wang and Xie (1998) used an intermediate anomaly model to show that some modes in the western Pacific warm pool were stable until the atmosphere model was coupled to an ocean model. Upon coupling, an unstable, MJO-like mode was generated.

More recently, there have been two studies in which coupled and uncoupled runs performed with the same atmospheric GCM (AGCM) were compared to determine whether coupling with an ocean model improved the simulated ISO. Waliser et al. (1999) made two AGCM integrations that were identical except for the inclusion of SST feedback. Both runs had as boundary conditions a specified annual cycle in SST, but in one run, the atmosphere was coupled to a slab mixed layer that predicted SST anomalies equatorward of 24° latitude. The SST perturbations were constrained to remain small so that effects of coupling were due to atmospheric interaction with the sea surface and not a change in the model's basic state. When an AGCM is coupled to an ocean model, the coupled model comes to some new basic state (i.e., the SST climatology and winds change). It cannot be known whether any change in the ISO noted upon coupling is due to direct interaction with the ocean or to the change in the basic state. Waliser et al. (1999) point out that there is currently no atmospheric model that has the same climatology as its coupled version.

In the run with interactive SSTs, Waliser et al. (1999) saw an improvement in the model's simulation of intraseasonal variability. The phase speed of the MJO disturbance in the eastern hemisphere was reduced, bringing it closer to observations, and the seasonality of the MJO improved, with an increase in the number of events occurring in boreal winter. The mechanism by which coupling improved the ISO simulation was that the positive SST anomaly east of the convection increased the meridional convergence into the region of low pressure to the east of the convection. Enhanced meridional convergence transported moisture into the region east of the convection, destabilizing the atmosphere there. The buildup of low-level moisture (and therefore moist static energy) east of existing convection and the consequent destabilization of the eastward-moving mode was more pronounced in the coupled run than in the fixed SST run. Although the model did generate reasonable fluxes of latent heat, these fluxes were less important in building up the low-level moisture in advance of convection than was the frictional convergence mechanism. An uncoupled form of this mechanism was first proposed by Wang (1988), who demonstrated the role frictional convergence plays in the selection of planetary scales in the ISO. Wang and Li (1994) presented a thorough analysis of this mechanism and compared it with wave–CISK (conditional instability of the second kind) (Lau and Peng 1987) and wind–evaporation feedback (Emanuel 1987; Neelin et al. 1988) mechanisms.

Hendon (2000) performed a similar experiment with the Geophysical Fluid Dynamics Laboratory AGCM coupled to a mixed layer ocean model. The coupled run was then compared to another run where the prescribed SSTs were those of the coupled-run climatology. This removed the effect of the change in basic state upon coupling, a problem pointed out by Waliser et al. (1999). In this experiment, the effects of coupling were minimal because the coupled model did not produce SST anomalies of sufficient magnitude. Hendon found that, while the model produced realistic surface shortwave radiation anomalies, they did not add constructively with the latent heat flux anomalies to form SST anomalies similar in magnitude to those observed. In addition, the latent heat flux anomalies were too weak and not spatially coherent. Hendon reasoned that the model was unable to produce the proper latent heat fluxes because the model did not produce mean westerlies in the western Pacific warm pool. Therefore, the phasing of surface westerlies relative to the enhanced convection was unrealistic. The different results of the experiments of Waliser et al. (1999) and Hendon (2000) point out the importance of an AGCM's climatology in the simulation of the ISO.

In summary, both observations and theoretical studies

suggest that we may need to model air–sea interactions to properly simulate the ISO. By their nature, observational studies do not easily yield information about causality, and the number of the GCM experiments on the effects of coupling on the ISO is still small. Another issue is that all of the modeling studies mentioned above concerned only the boreal winter Madden–Julian mode of the ISO. The summertime ISO is marked by a weakening of the eastward-moving equatorial MJO mode, and a strengthening of northward-moving modes. In the Asian monsoon onset season of May–June, the ISO shows pronounced northward propagation in the Indian Ocean (e.g., Yasunari 1979; Krishnamurti and Subrahmanyam 1982; Hartmann and Michaelson 1989), while in the August–October season, the ISO shows westward and northward movement in the western Pacific as well as a northward-moving Indian Ocean component (Murakami et al. 1984; Nitta 1987; Wang and Rui 1990; Kemball-Cook and Wang 2001). The existence of these additional modes in summer creates a very rigorous test for a GCM. To reproduce the summertime ISO, a GCM must simulate the seasonal changes in the mean flow, and westward and northward as well as eastward movement of the convection and circulation anomalies, in addition to any air–sea interactions that may exist.

The goal of this project is to address the question of whether coupled atmosphere–ocean models are required to reproduce the observed tropical intraseasonal variability, and to examine the nature of air–sea interaction in the boreal summer intraseasonal oscillation. The method used is to compare three GCM runs. The first is an Atmospheric Model Intercomparison Project (AMIP) (Gates 1992) integration in which an AGCM is run with specified monthly mean SSTs and sea ice as the lower boundary forcing. In the second simulation, the same AGCM is coupled to the University of Hawaii intermediate 2.5-layer ocean model (Wang et al. 1995). In the third run, the SST climatology generated in the coupled run is used to create monthly mean SSTs, which are then used to drive the AGCM in an uncoupled configuration similar to the AMIP run. The three runs are abbreviated AMIP, CPL, and CPLDBS hereafter. By comparing the three runs with data from the NCEP reanalysis and National Oceanic and Atmospheric Administration (NOAA) outgoing longwave radiation (OLR) data, we can assess the importance of the interactive sea surface, and separate out its effects from those of the change in basic state, which occurs upon coupling.

In a departure from previous studies, we will focus on the ISO in boreal summer. The studies of Kemball-Cook and Wang (2001), Annamalai and Slingo (2001, hereafter AS01), and Lawrence and Webster (2001) have provided an observational benchmark for diagnosis of the model ISO in boreal summer. The experiments of Waliser et al. (1999) and Hendon (2000) and also the observations of the MJO and BSISO point out the importance of the model's reproducing reasonable latent heat flux anomalies. This will be particularly important in the BSISO, in which meridional frictional convergence onto the equator plays a lesser role as convection moves northward away from the equator toward India.

The rest of the paper is organized as follows: section 2 is a description of the models used in this study and of the methods used to filter the data and to diagnose the results. Section 3 is a description of the climatologies of the coupled and uncoupled runs. In section 4, we will briefly describe the model's winter MJO mode for the purpose of comparison with the studies of Waliser et al. (1999) and Hendon (2000). In section 5, the model simulations of the ISO in May–June are discussed, and, in section 6, we examine the August–October ISO. In section 7, we discuss the results and present some conclusions and directions for future work.

## 2. Method

### *a. Model description*

The atmospheric model used in this study is the ECHAM-4 AGCM (Roeckner et al. 1996). The model is run at T30 resolution and has 19 layers in the vertical; approximately 5 of these lie within the planetary boundary layer. The convection scheme used is that of Tiedtke (1989) with modifications to the closure assumption, which ties the cloud-base mass flux to convective instability rather than moisture convergence. The Tiedtke scheme treats shallow, midlevel, and penetrative convection, and includes convective downdrafts. The prognostic cloud-water scheme of Sundqvist (1978) is used.

The University of Hawaii 2.5-layer ocean model was originally developed by Wang et al. (1995), and implemented by Fu and Wang (2001), and consists of two active upper-ocean layers overlying a deep inert layer. There is a mixed layer and a thermocline layer, and both are allowed to vary in depth. The model includes Seager–Zebiak–Cane model dynamics (1988) integrated with Niiler–Kraus' (1977) mixed layer physics. The ocean model requires as input the insolation, surface winds, and cloud cover. The surface winds affect the mixed layer temperature through turbulent entrainment, surface evaporation, sensible heat flux, and temperature advection by wind-induced currents. The cloudiness influences the mixed layer temperature by affecting shortwave and longwave radiation fluxes and by changing the entrainment rate associated with the mixing process. The surface winds also affect the mixed layer temperature by inducing upwelling and thus changing the mixed layer depth. The University of Hawaii 2.5-layer ocean model, when coupled to the ECHAM-4 AGCM, produces a coupled run free of climate drift over a 25-yr integration, and has a reasonable SST climatology (discussed in section 3a).

### *b. Observations and filtering*

Two datasets provide observations against which to compare the model results. They are interpolated daily

average maps of OLR from NOAA polar-orbiting satellites (Liebmann and Smith 1996) and daily average fields from the National Centers for Environmental Protection–National Center for Atmospheric Research (NCEP–NCAR) reanalysis (Kalnay et al. 1996). Fifteen years of data were used, extending from 1983 to 1997. The model simulations are 15 years in length.

The OLR, reanalysis, and model output fields were filtered in the same manner using a bandpass filter, which retains variability in the 10–100-day band. The filter was constructed as follows: first, the annual cycle and its first three Fourier harmonics were removed from the daily mean fields. Next, the interannual variability was removed using the method of Rui and Wang (1990). Finally, a running pentad mean was applied to remove high-frequency (<10 days) variability.

### c. Compositing method

In order to compare the model ISO with the observed ISO, we form composite ISO events for all three model runs and for the observations using the method of Kemball-Cook and Wang (2001). The ISO events were identified by their convective signal, as measured by the OLR anomaly. Separate composites were formed for three seasons: winter (November–March), May–June (MJ), and August–October (AO). The mean climatology undergoes a shift from early to late boreal summer, as does the character of the ISO (Kemball-Cook and Wang 2001). July is a time of transition between early and late summer and was excluded from the study.

Because of the different propagation modes present in the ISO (Zhu and Wang 1993; Wang and Rui 1990), care is required in forming the composite. In order to form a composite that captures the eastward-moving convective envelope and still retains the possibility of westward and northward movement within an ocean basin, we require a given convective event to have a large-scale signal in the Indian Ocean and subsequently (no more than 20 days later) in the western Pacific. We do not specify the direction the convection must travel *within a given ocean basin*, only that there be a large-scale convective envelope that is generally eastward moving. The convective signal was measured by the filtered OLR anomaly averaged over the boxed base regions in Fig. 1a. If the OLR anomaly averaged over each box was less than $-15$ W m$^{-2}$ as the ISO event passed overhead, the event was a possible candidate for the composite.

The Indian Ocean base region was chosen because it is within this area that equatorial ISO convection is found most frequently (Wang and Rui 1990). The western Pacific base region was chosen because it is a region of large intraseasonal OLR variance and high SST for all seasons. The winter and MJ composites are centered in time around the day on which the convective anomaly averaged over the Indian Ocean base region reaches its maximum intensity (i.e., OLR is at a minimum). The AO composite is centered around the day on which the convective anomaly averaged over the western Pacific base region reaches its maximum intensity. While centering the AO composite around the Indian Ocean base region does not change the basic features of the composite, its statistical significance is reduced. This is because the lengths of each ISO event are slightly different, and there is more variability in event length for AO than in winter and MJ. Figure 1 shows an example of event selection for the observed OLR during the 1995 May–June season.

The OLR averaged over the Indian Ocean and western

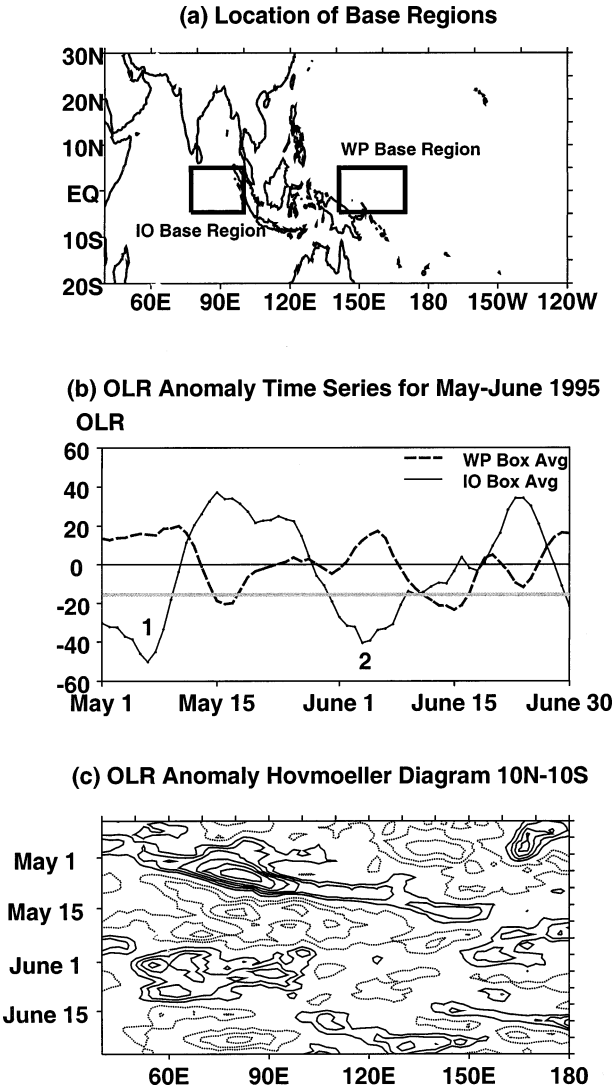


FIG. 1. Compositing procedure. (a) Location of base regions used to form the composites. (b) Example of event selection. OLR anomaly time series for May–Jun 1995. Dashed line shows the OLR anomaly averaged over the Indian Ocean base region shown in (a). Solid line shows the OLR anomaly averaged over the western Pacific base region shown in (a). (c) OLR anomaly Hovmoeller diagram for 10°N–10°S. Solid (dashed) contours are negative (positive) OLR anomaly (W m$^{-2}$). First contour is at 10 W m$^{-2}$, and contour interval is 10 W m$^{-2}$.

Pacific base regions (Fig. 1a) shows two candidate events for which the Indian Ocean and western Pacific base region averaged OLR minima were less than −15 W $m^{-2}$ and out of phase with one another (Fig. 1b). Therefore, for 1995, the events to be included in the MJ composite had OLR minima (labeled ''1'' and ''2'' in Fig. 1b) over the Indian Ocean base region on 7 May and 3 June. A Hovmoeller diagram for the latitude belt 10°N–10°S (Fig. 1c) shows the OLR anomaly for this time period. The two events show that the convection associated with the ISO intensifies over the Indian Ocean, dissipates somewhat as the anomaly passes over the Maritime Continent, and then reintensifies as it moves over the western Pacific warm pool.

The statistical significance of the composited fields was assessed using Student's t-test, after first applying the *F* test to determine that the use of the *t* test was appropriate (Press et al. 1986). The null hypothesis used to test the significance of the composites was that there are no coherent anomalies in the 10–100-day band. To test this hypothesis, a synthetic composite was constructed using an ensemble of events whose members had an anomaly value of zero throughout the domain. This synthetic composite had the same number of members as the real composites.

## 3. Comparison of the AMIP and CPL run climatologies

### *a. Seasonal mean fields*

We turn first to the mean climate simulated in the coupled (CPL) and uncoupled (AMIP) model runs, comparing the model climatologies to those of the NCEP reanalysis and NOAA OLR data. Given the simulated basic states of the two model runs, how well can we expect the models to reproduce the ISO, in both summer and winter? We will look at the seasonal cycle of several key variables, focusing on the eastern hemisphere Tropics, 30°N–30°S and 0°–150°W.

Accurate representation of the SST distribution is critical for a model's simulation of deep convection, which is a key component of the ISO. The statistical threshold for deep convection is 300 K (Graham and Barnett 1987). We compare the SST climatology produced by the coupled run with that of the reanalysis skin temperature (Fig. 2). The AMIP run uses monthly mean observed SSTs (Gates 1992), which are similar to the reanalysis. In boreal winter, the reanalysis shows SST maxima in the western Pacific warm pool and west of Sumatra in the Indian Ocean. The regions of warmest water lie on or south of the equator. The CPL model SST climatology does a reasonably good job of locating the 300-K contour, but does not capture the regions of maximum SST in the eastern Indian Ocean or the western Pacific warm pool, and is too warm over southern India. In May–June, the situation is similar. Though the model is able to capture the region where the SST > 300 K, it has a cold bias that is especially pronounced in the western Pacific warm pool, and is also notable in the Indian Ocean. In August–October, the model is too cool over most of the western Pacific and the Indian Ocean. Though the model does detect the presence of cold water upwelling off Somalia, this feature extends too far eastward into the Indian Ocean. In the reanalysis, this feature remains coastally trapped. In summary, the model does a reasonable job with the 300-K contour, but has a cold bias in the Indian Ocean and the western Pacific warm pool.

In the coupled model, this cold bias is likely a result of interaction between the atmosphere and the ocean. In the AMIP run, the equatorial zonal winds over the western Pacific have an easterly bias compared with those of the NCEP reanalysis. If the ECHAM model is coupled with a perfect ocean model, then the easterly bias in the atmosphere model will cool down the ocean because of the increase of the total wind speed (stronger easterlies). The cooling of the ocean will in turn enhance easterlies along the equator to the west of the cooling region. This is a positive feedback, which would amplify the original model bias. This means that as long as the AGCM is not perfect, air–sea coupling might amplify the bias, while inducing an accompanying bias in SST, provided there is a positive air–sea feedback. Thus, the cold bias is caused by a bias originally found in the AGCM winds, and is amplified through air–sea interaction, yielding a cold bias in SST. The cold bias in the CPL run SSTs means that the coupled model basic state is less conducive to deep convection, which is an integral part of the ISO.

The impact of the SST distribution can be clearly seen in the seasonal mean OLR patterns (Fig. 3). In winter, CPL shows far less convection than is observed in the equatorial western Pacific, where the model's SST cold bias is most pronounced. The AMIP run, which is driven with observed SSTs, does a better job in the western Pacific, though it also misses the eastward extension of the ITCZ and generates convection too far to the west in the equatorial Indian Ocean. Note that the convection pattern over the Maritime Continent is more realistic in the CPL run than in the AMIP run.

In May–June, the main difference between the AMIP and observed OLR climatologies is the lack of convection over India and southeast Asia in the AMIP run. The ECHAM-4 model has been shown to produce a weak Asian monsoon (Roeckner et al. 1996). The CPL run shows some improvement in the simulation of the diabatic heating associated with the monsoon. Both CPL and AMIP model runs underestimate convection in the Bay of Bengal, though CPL is somewhat closer to the observations. In the western Pacific, CPL produces only weak convection along 7°N and the extension of convection along the South Pacific convergence zone (SPCZ), seen in the observations and the AMIP run, is completely absent.

In AO (Fig. 4), the AMIP simulation underestimates

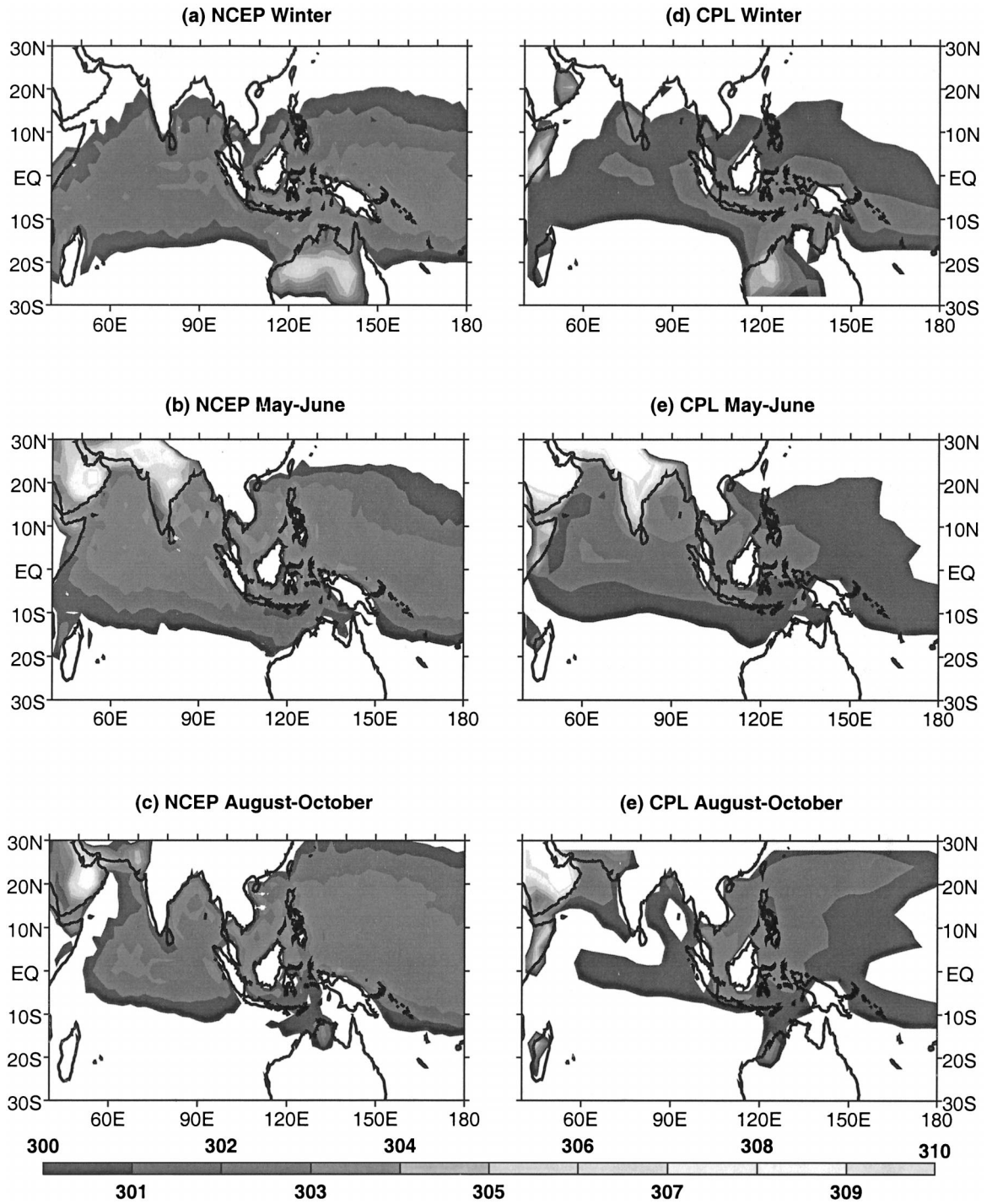


FIG. 2. Seasonal mean surface temperature (K). The contour interval is 1 K, with the first contour at 300 K. (a) NCEP reanalysis winter mean skin temperature. (b) NCEP reanalysis May–Jun mean skin temperature. (c) NCEP reanalysis Aug–Oct mean skin temperature. (d) CPL mean winter surface temperature. (e) CPL May–Jun mean surface temperature. (f) CPL Aug–Oct mean surface temperature.

the northward movement of the mean convection over the Indian subcontinent and southeast Asia, and convection in the Bay of Bengal is nearly absent. The CPL run does better, although the heat source over the Asian landmass is still less intense than is observed. Both model runs locate the ITCZ too far to the north, and the CPL integration, with its western Pacific cold bias, again underestimates the convection along the equator and the SPCZ.

Figure 5 shows the seasonal mean 1000-mb zonal

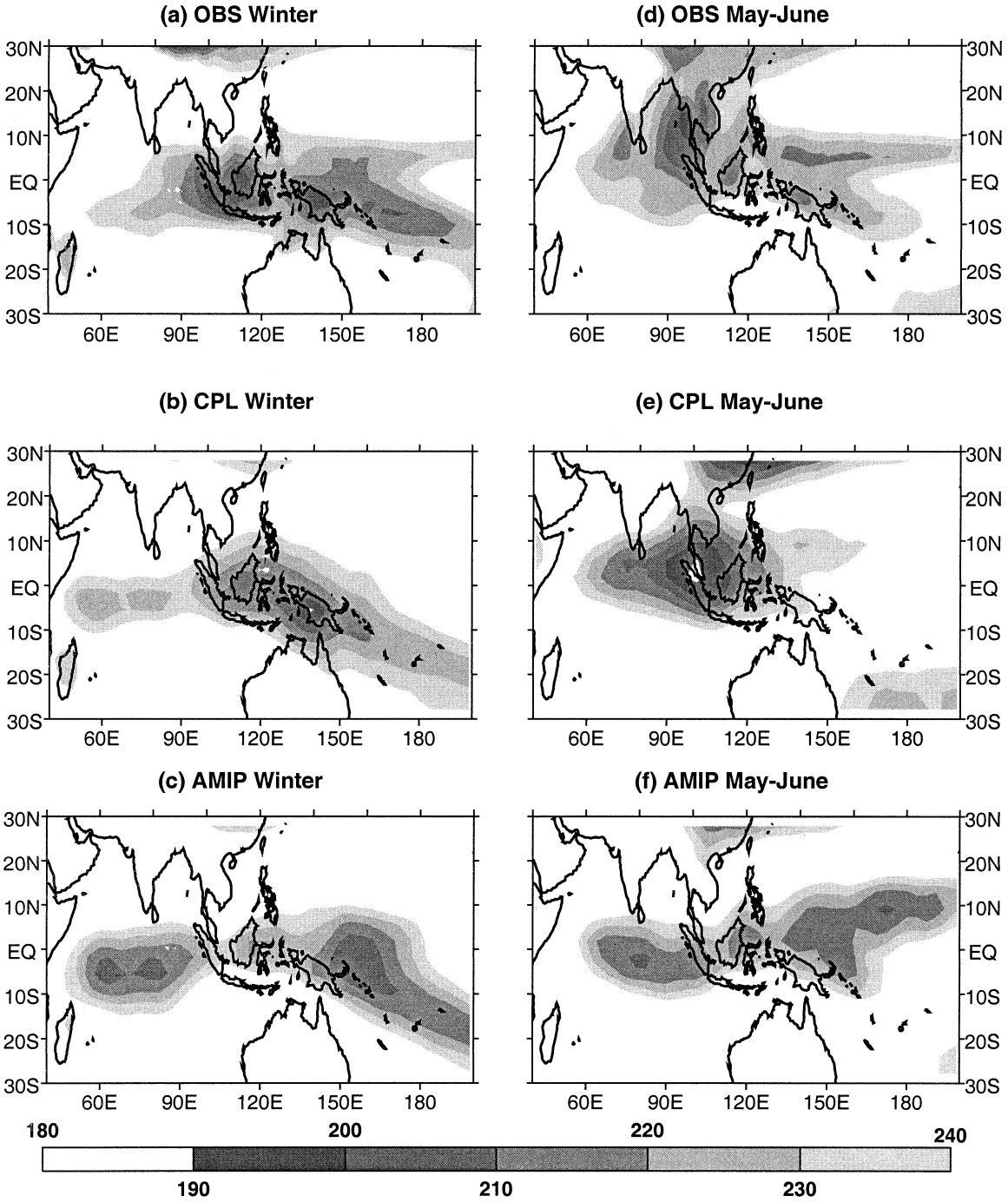


FIG. 3. OLR (W m$^{-2}$) seasonal averages for winter and May–Jun. First contour is at 240 W m$^{-2}$. (Only regions of mean deep convection are shown.) Contour interval is 10 W m$^{-2}$. (a) Observed winter OLR. (b) CPL winter OLR. (c) AMIP winter OLR. (d) Observed May–Jun OLR. (e) CPL May–Jun OLR. (f) AMIP May–Jun OLR.

wind fields. In winter, the CPL run does a good job of simulating the wind field pattern in the Indian Ocean, though it slightly underestimates the magnitude of the wind. Unlike the reanalysis, however, CPL does not have a region of westerlies extending into the western Pacific. This is critical, because it means that the region of convergence along the SPCZ is missing, and convection associated with the ISO is known to be concentrated in the mean convergence zones. The AMIP run gives a better simulation of the 1000-mb zonal wind in the western Pacific, and this is consistent with the stronger OLR signal found in AMIP. In MJ, both model

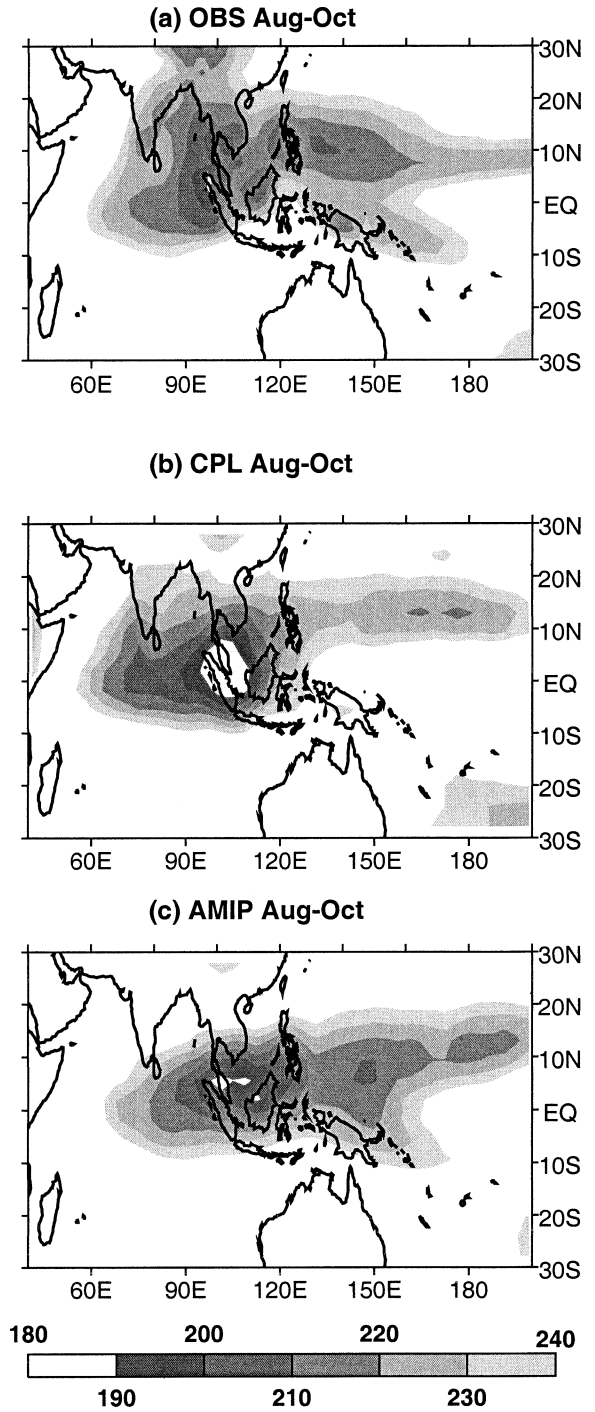


FIG. 4. OLR (W $m^{-2}$) seasonal averages for Aug–Oct. First contour is at 240 W $m^{-2}$. (Only regions of mean deep convection are shown.) Contour interval is 10 W $m^{-2}$. (a) Observed Aug–Oct OLR. (b) CPL Aug–Oct OLR. (c) AMIP Aug–Oct OLR.

runs do a good job of simulating the 1000-mb zonal wind in the Indian Ocean. In CPL, the easterlies intrude too far to the east equatorial and northern west Pacific. This problem persists in AO in the CPL run (not shown).

To summarize, the CPL and AMIP model runs simulate a more realistic mean state in winter than in summer. Only in winter do they correctly simulate the basic shape of the region of deep convection. The fact that the AMIP run has deficiencies in its mean OLR field suggests that they fail in simulating the distribution of OLR for reasons other than simply that the SST is wrong; difficulties in simulating the low-level wind field and convergence zones play a role, as well.

### *b. Intraseasonal variability*

In this section, we examine the impact of coupling on the simulated intraseasonal variability. Waliser et al. (1999) noted an increase in the number of ISO events upon coupling, with the largest increase occurring in boreal winter. Table 1 summarizes the number of events occurring in each season for each integration. We see an increase in wintertime ISO activity in the coupled run, though the increase is smaller than was seen by Waliser et al. (1999). The number of events rose from 22 in the AMIP run to 27 in the CPL run, from 11 to 14 in MJ, and no change for AO. These increases in winter and MJ reflect the increased variability in the ISO band in the CPL run (discussed below). The CPLDBS experiment has the smallest number of ISO events of all three runs. This is consistent with the reduction in SSTs in CPL and the loss of the any strengthening of the ISO signal that coupling affords. The reduction in ISO variability suggests that the coupled-run basic state is less conducive to deep convection. The coupling gives extra strength to the ISO and overcomes the less conducive basic state to give the CPL run stronger intraseasonal variability than in the AMIP run.

To further assess changes in the model's intraseasonal variability upon coupling, we examine the space–time spectra of the filtered OLR for the full year and compare them to observations (Fig. 6). The space–time spectra (Hayashi 1982) were calculated and averaged over the 5°N–5°S latitude band. The observed OLR anomaly spectrum has a maximum at eastward-moving wavenumber 2 between 30 and 60 days, consistent with previously reported characteristics of the ISO (Madden and Julian 1994). This broad maximum reflects the variability in period at interannual (Slingo et al. 1999) and seasonal (Hartmann et al. 1992) timescales. As in the observations, the AMIP run shows more variability in eastward-moving than westward-moving waves, but the peak is far more diffuse than that of the observations. The peak falls at a higher wavenumber in AMIP than in the observations, suggesting that the intraseasonal variability is weaker than observed and is too broad in its spatiotemporal scale.

In the coupled run, the power tends to consolidate at lower eastward wavenumbers than in AMIP, and is closer to the observations in intensity. There is a reduction in high-frequency variability in CPL, which brings it into closer agreement with the observed spectrum. The peak is, however, still concentrated at wavenumbers and

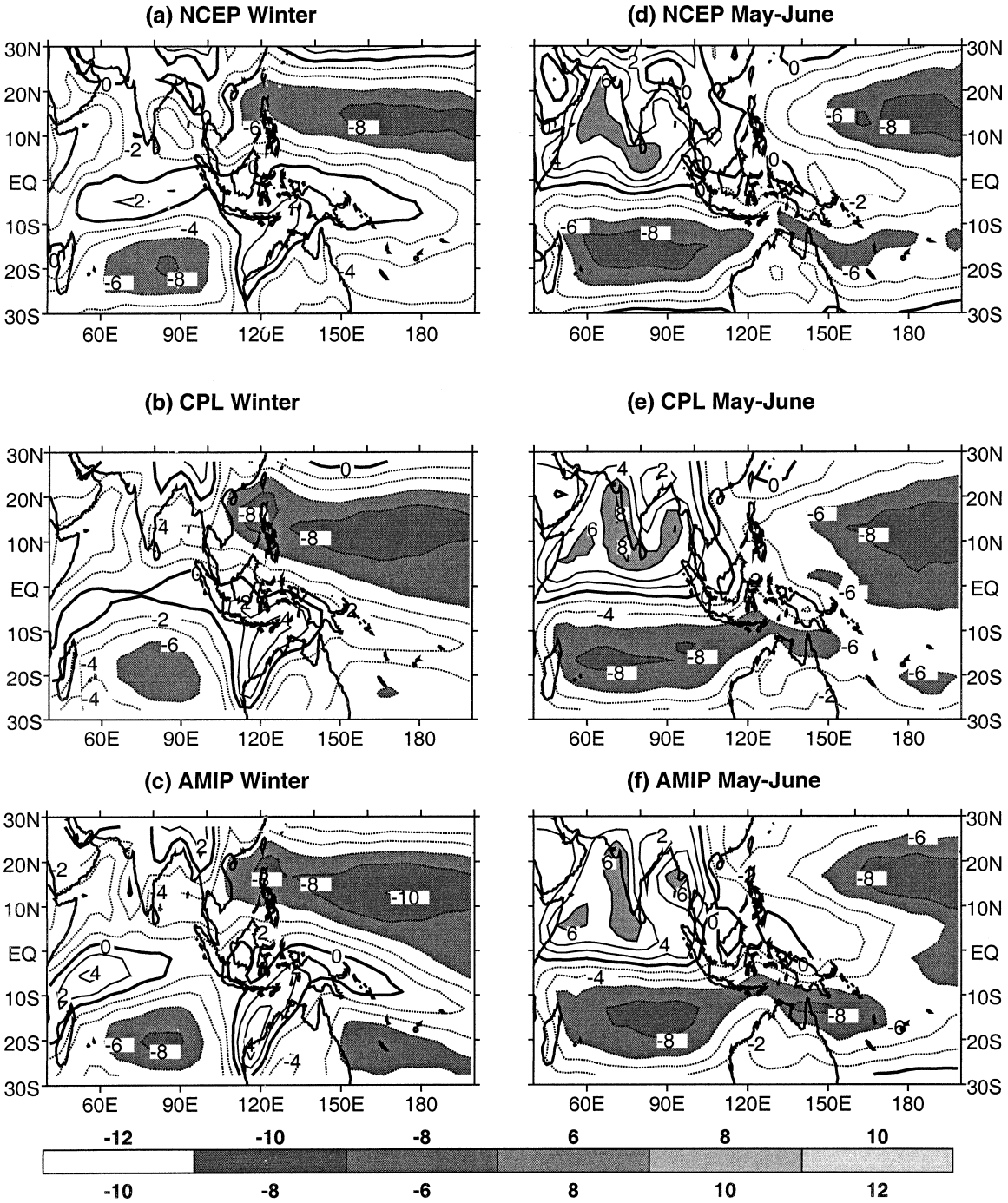


FIG. 5. The 1000-mb zonal wind seasonal averages for winter and May–Jun. First contour is at 2 m $s^{-1}$. Contour interval is 2 m $s^{-1}$. Solid (dashed) contours indicate westerly (easterly) winds. Zero line is the thick solid contour. (a) NCEP reanalysis winter $u$(1000 mb). (b) CPL winter $u$(1000 mb). (c) AMIP winter $u$(1000 mb). (d) NCEP reanalysis May–Jun $u$(1000 mb) (e) CPL May–Jun $u$(1000 mb). (f) AMIP May–Jun $u$(1000 mb).

periods that are too high. Coupling also changes the westward wave spectrum significantly; the intensity is more realistic (reduced at 60 days), and the range of periods is narrowed. Thus, coupling enhances eastward propagation while reducing westward propagation. This produces a sharper asymmetry between eastward and westward propagation, as in the observations (Fig. 6a). In this sense, coupling makes the overall spectrum more realistic.

The spectrum for the CPLDBS case falls in between the AMIP and CPL cases. A more consolidated peak is produced but it is not as intense or as coherent as in

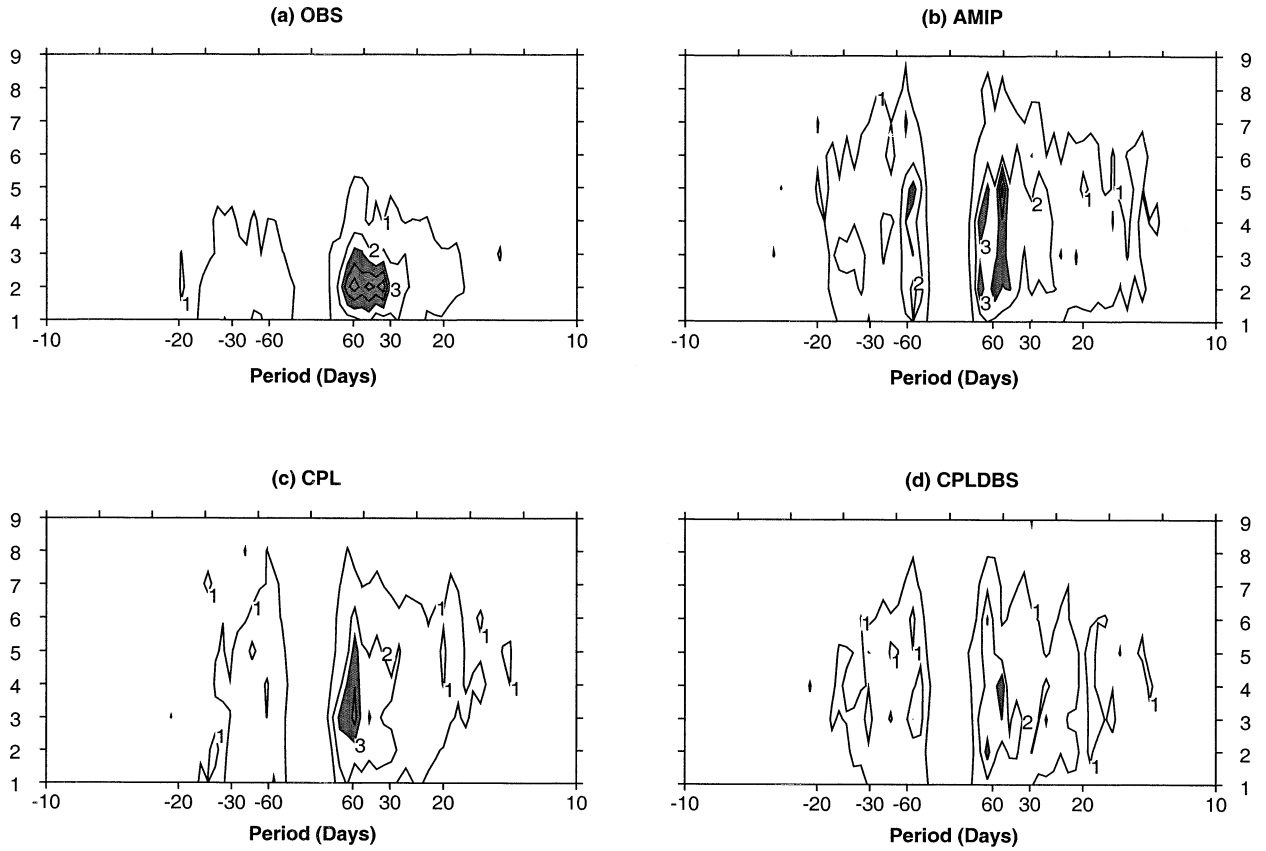


FIG. 6. Wavenumber period spectrum for the full year, averaged in latitude from 5°S to 5°N. Vertical axis is wavenumber and horizontal axis is period (days) Positive (negative) periods denote eastward (westward) moving waves. Contour interval is 1 (W $m^{-2}$)$^2$, with the first contour at 1 (W $m^{-2}$)$^2$. Regions where power is greater than 3 (W $m^{-2}$)$^2$ are shaded. (a) Observed OLR spectrum. (b) AMIP. (c) CPL. (d) CPLDBS.

CPL. Results for circulation variables and also for individual seasons and the latitude belt 10°–15°N (not shown) are similar to those presented in Fig. 6, with the CPL spectrum looking the most realistic of the three model runs.

## 4. Boreal winter ISO

The observed ISO is strongest during the November–March season and reaches its maximum intensity near the equator. For the purpose of comparison with the results of Waliser et al. (1999), Hendon (2000), and numerous observational studies, we begin the analysis of the composite with a look at the eastward propagation of the convection and circulation anomalies along the equator in boreal winter.

TABLE 1. Number of ISO events per season for each integration.

| Run | Winter | May–Jun | Aug–Oct |
|---|---|---|---|
| AMIP | 22 | 12 | 11 |
| CPL | 25 | 13 | 11 |
| CPLBS | 10 | 5 | 6 |

Figure 7 shows Hovmoeller diagrams of anomalies of OLR and 1000-mb zonal wind averaged across the equatorial belt. The observations show an eastward-propagating disturbance in OLR accompanied by easterly low-level wind anomalies located to the east of the convection and westerly anomalies to its west, as viewed from a fixed location. This result is consistent with other observational studies (e.g., Madden and Julian 1972; Wang and Rui 1990; Hendon and Salby 1994). The structure of the zonal wind anomaly implies low-level convergence preceding the convection and low-level divergence following it, in agreement with the observational results of Hendon and Salby (1994) and Maloney and Hartmann (1998). Low-level convergence preceding the convection is a fundamental characteristic of frictional convergence, a mechanism that allows conversion of available potential energy to kinetic energy (instability) and sustains the intraseasonal disturbance against dissipation (Wang 1988; Hendon and Salby 1994). The OLR anomaly reaches a minimum in the Indian Ocean (this may be an artifact of the compositing method, which centers the composite around the time of maximum convection in the Indian Ocean) and shows

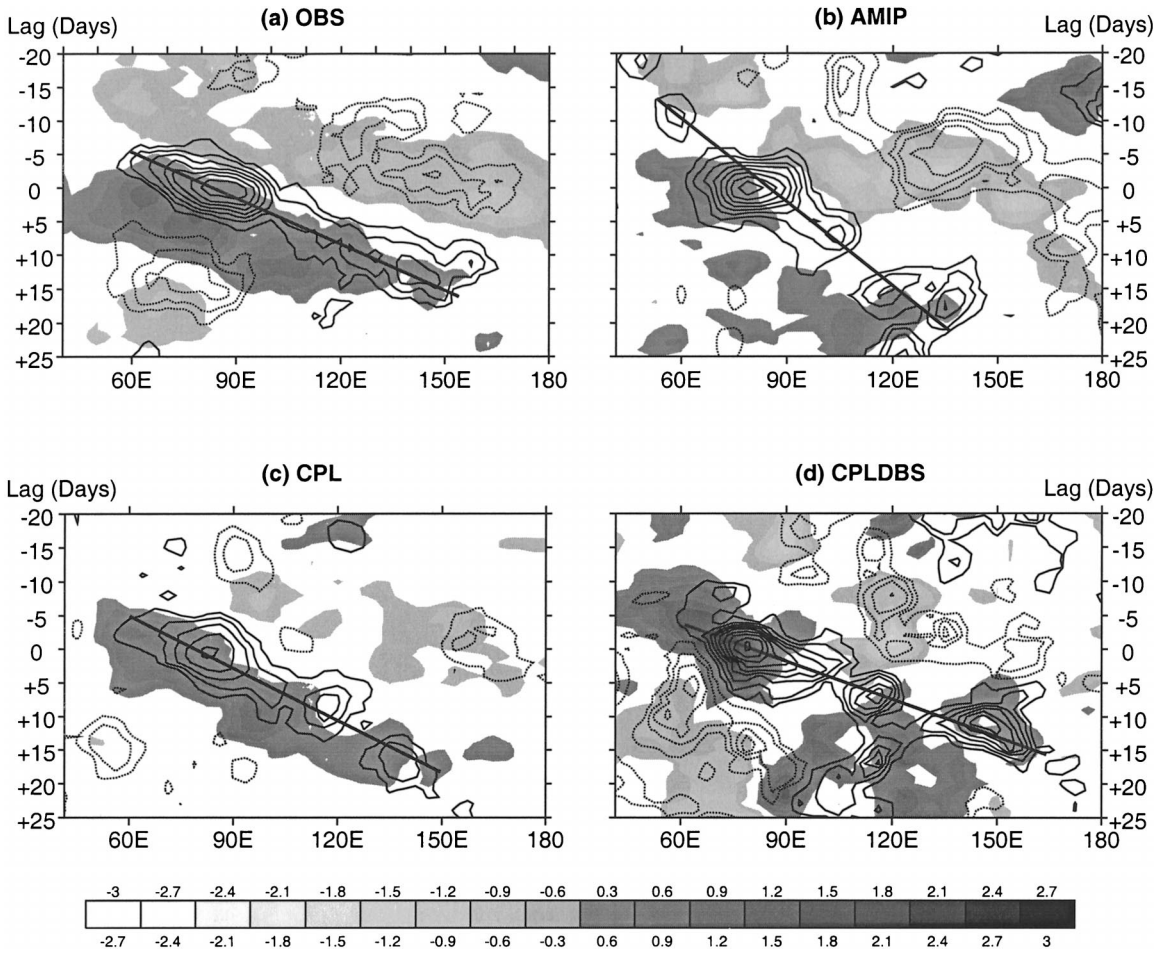


FIG. 7. Composite winter OLR and 1000-mb zonal wind anomaly Hovmoeller diagram for 10°N–10°S. Horizontal axis is longitude. Vertical axis is time (days) relative to day 0 of the composite. Only contours significant at the 90% level are shown. Solid (dashed) contour lines are negative (positive) OLR (W $m^{-2}$) anomaly corresponding to enhanced (suppressed) convection. Shaded contours are 1000-mb zonal wind anomaly (m $s^{-1}$). (a) Observed. (b) AMIP. (c) CPL. (d) CPLDBS.

coherent propagation across the Maritime Continent into the western Pacific. The OLR anomaly decays as it reaches the colder water near the date line.

Wang and Xie (1998) showed that coupling reduces the eastward propagation speed for equatorial eastward-propagating moist Kelvin waves and reduces westward propagation for off-equatorial westward-propagating moist Rossby waves. This is because the ocean response takes a longer time to feedback to the atmosphere. The modeling study of Waliser et al. (1999) showed a similar result, with coupling slowing the eastward propagation of the ISO disturbance. Here, we qualitatively compare phase speeds of the ISO in the CPL and CPLDBS runs, because they have the same background SST climatology. In CPLDBS, the eastward propagation is faster, implying that the coupling does slow down the eastward propagation of the ISO, as in the two studies noted above.

The AMIP convective anomaly is apparent over the Indian Ocean, but disappears while passing over the Maritime Continent, reappearing once more in the western Pacific. In the AMIP run, the ISO shows some characteristics of the seesaw oscillation between the Indian Ocean and the western Pacific described by Zhu and Wang (1993). The CPL run, meanwhile, has an OLR anomaly that is less intense than that of the AMIP run, but is more coherent, showing continuous propagation from the Indian Ocean across the Maritime Continent into the western Pacific. The low-level wind anomaly in AMIP is not as coherent with the convection as it is in the reanalysis. The CPL low-level westerly wind anomaly is more closely linked with the OLR anomaly, as in the reanalysis, although the easterlies east of the convection are too weak.

The CPLDBS run is the most intense of the three model runs, and is also the noisiest. This is in part due to the fact that the CPLDBS composite contains the fewest events, but examination of individual events from all three runs shows that CPLDBS events are not as well organized as those of CPL and AMIP. To test

that the improvement in coherence in going from CPLDBS to CPL or AMIP was not simply a function of fewer events in CPLDBS, we recreated the AMIP and CPL OLR composites using a random sample of 10 events (the same number used to form the CPLDBS composite). The coherence and overall structure of the AMIP and CPL composites were unchanged as a result of reducing the number of composited events (not shown). We conclude from this test that the increased noise in CPLDBS is not an artifact of the compositing procedure, but reflects the same reduction in intraseasonal variability displayed in Fig. 6d.

The CPLDBS wind anomaly does not smoothly cross the Maritime Continent, and a westward-moving convective component is observed in the western Pacific (as in AMIP); this feature is present neither in CPL nor in the reanalysis. We can conclude from Fig. 7 that coupling does improve the modeled simulation of the ISO during boreal winter.

In winter, the CPL run shows SST anomalies of similar overall character and the same order of magnitude as the observations in the Indian Ocean basin (Fig. 8). Both negative and positive SST anomalies are reasonably well simulated. However, in the western Pacific, the positive anomaly preceding the convection is too weak. This fact, taken together with the weak and disorganized easterlies in Fig. 7, suggest that the CPL run is not simulating the suppressed phase of the ISO well in the western Pacific.

Figure 9 shows the contributions of the shortwave radiative flux and the latent heat flux, which make up most of the net surface heat flux. We compare the model-run fluxes with those of the NCEP reanalysis. Despite known difficulties with the reanalysis surface fluxes (e.g., Shinoda et al. 1999), we use these fluxes to give an order of magnitude estimate of the real surface fluxes as a gross check on the accuracy of the modeled surface fluxes. Our primary concern here is to examine the coherence and relative strengths of the modeled latent and shortwave fluxes.

In both CPL and AMIP model runs, the surface heat flux into the ocean is dominated by the shortwave radiative flux. This is particularly true in CPL, in which weak easterly winds in the western Pacific cause a weak latent heat flux there. In the reanalysis, the contributions of the latent and shortwave fluxes are more nearly equal. One may ask then how a reasonable ISO anomaly can be simulated by CPL, which produces a reasonable OLR anomaly despite poorly simulated surface fluxes. In both model runs, convection is controlled primarily by low-level convergence, which is twice as strong in the model as in the reanalysis. Waliser et al. (1999) found that low-level moistening contributing to deep convection came primarily from convergence, and not from the surface fluxes, and this is consistent with what we see here. In the ECHAM-4 model runs, the latent heat fluxes are weaker than those of the reanalysis, and are not spatially consistent with the buildup of moisture prior to onset of convection. Instead, low-level convergence is better correlated with moisture buildup. The total heat flux is similar in CPL and the reanalysis, so that the model produces reasonable SST anomaly magnitudes. In the theoretical analysis of Wang and Xie (1998), the model includes two feedback processes. One is evaporation–wind–SST feedback through the changing latent heat flux and the other is cloud–radiation–SST feedback through the shortwave flux. Wang and Xie showed that both processes are positive feedback processes, which can lead to the unstable growth of the ISO (in reality, this growth can sustain the ISO against dissipation and enhance the ISO signal). This means that the two feedback mechanisms differ physically but their impacts on ISO are qualitatively the same.

## 5. The May–June ISO

The unique features of the boreal summer ISO are pronounced northward propagation of convection and circulation anomalies in the Indian Ocean during MJ (Yasunari 1979; Krishnamurti and Subrahmanyam 1982; Hartmann and Michaelson 1989) and northwestward propagation in the western Pacific during AO (Chen and Murakami 1988). These modes coexist with the eastward-propagating equatorial mode, which is weaker in summer than in winter (Wang and Rui, 1990). We first look at northward propagation in MJ, then northwestward propagation in AO.

Figure 10 shows Hovmoeller diagrams for the longitude range 65°–95°E, which is a region of pronounced northward ISO propagation. Several diagnostic studies (Kemball-Cook and Wang 2001; Lawrence and Webster 2001; AS01) have shown northward propagation of both enhanced and suppressed convective anomalies, with a band of low-level convergence leading the enhanced convective anomaly northward until approximately 5°N. Northward of 5°N, the convergence and convection anomalies are in phase. In addition to its strong northward propagation, the convective anomaly also shows weaker southward propagation. The MJ ISO, therefore, has the form of an eastward-moving equatorial convective anomaly undergoing asymmetric Rossby wave emanation (Kemball-Cook and Wang 2001; Lawrence and Webster 2001).

The coupled OLR anomaly shows some evidence of northward propagation and very weak southward emanation. The AMIP run, on the other hand, shows a primarily equatorial response, although there is some weak poleward movement. The convergence field in CPL has the northward-moving branch seen in the observations and also a southward-moving branch. The AMIP run does not have a northward-moving convergence anomaly. Note that the convergence in CPL is much stronger than in the observations. The CPLDBS run is similar to the AMIP run, with convection primarily centered on the equator and some weak southward propagation.

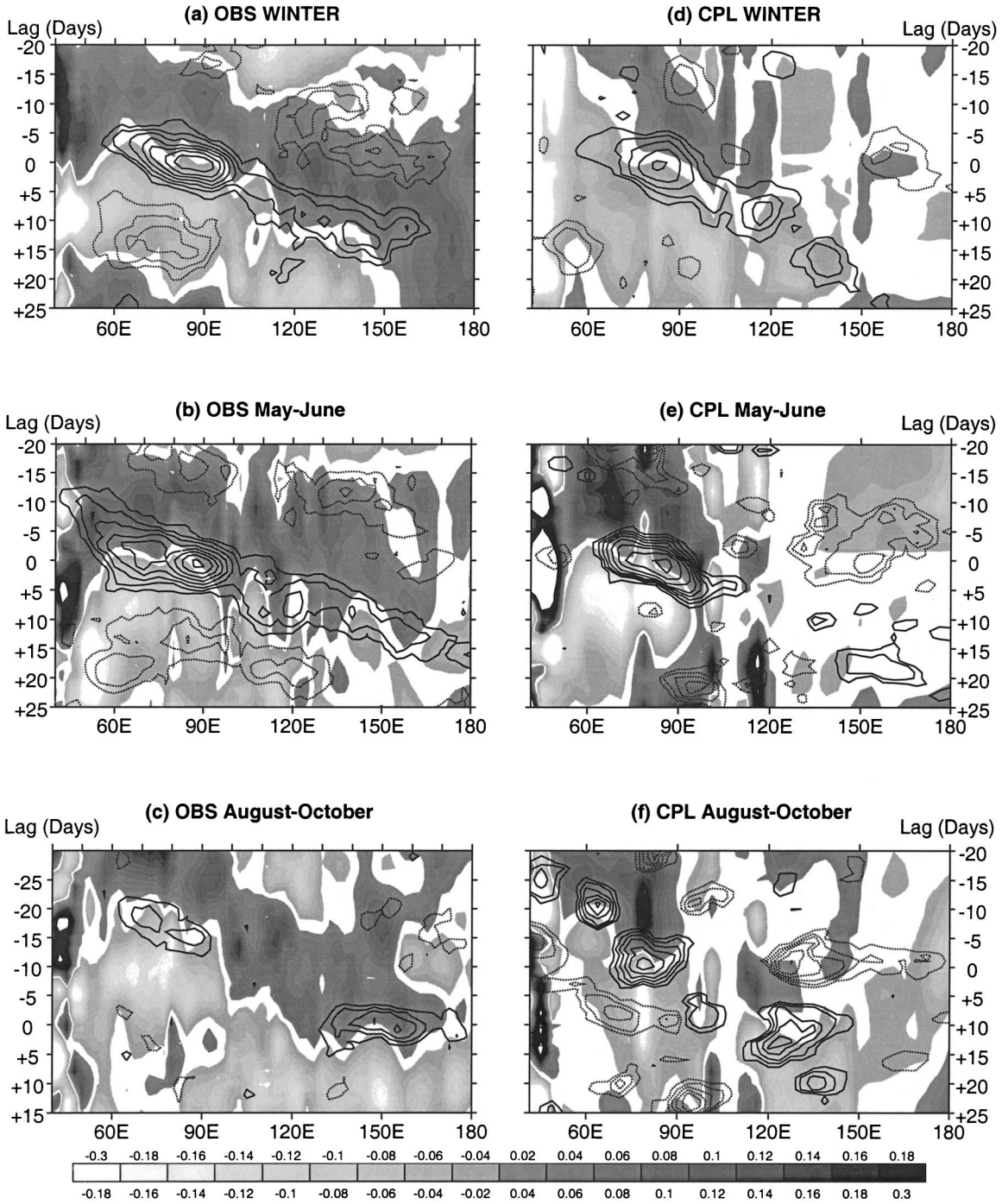


FIG. 8. Composite winter OLR and SST anomaly Hovmoeller diagram for 10°N–10°S. Horizontal axis is longitude. Vertical axis is time (days) relative to day 0 of the composite. Only contours significant at the 90% level are shown. Solid (dashed) contour lines are negative (positive) OLR (W $m^{-2}$) anomaly corresponding to enhanced (suppressed) convection. Shaded contours are SST (K). (a) Observed winter. (b) Observed May–Jun. (c) Observed Aug–Oct. (d) CPL winter. (e) CPL May–Jun. (e) CPL Aug–Oct.

Figure 11 is a comparison of MJ SST, latent heat flux, and convergence in the NCEP reanalysis and in the model runs. The reanalysis shows northward-moving zonal wind anomalies consistent with the convergence field. The latent heat flux anomaly is tightly coupled to the wind anomaly, with a northward-moving negative anomaly followed by a positive anomaly that builds in once the wind anomaly shifts to westerlies.

The CPL run captures the northward propagation in the zonal wind field and the positive latent heat flux

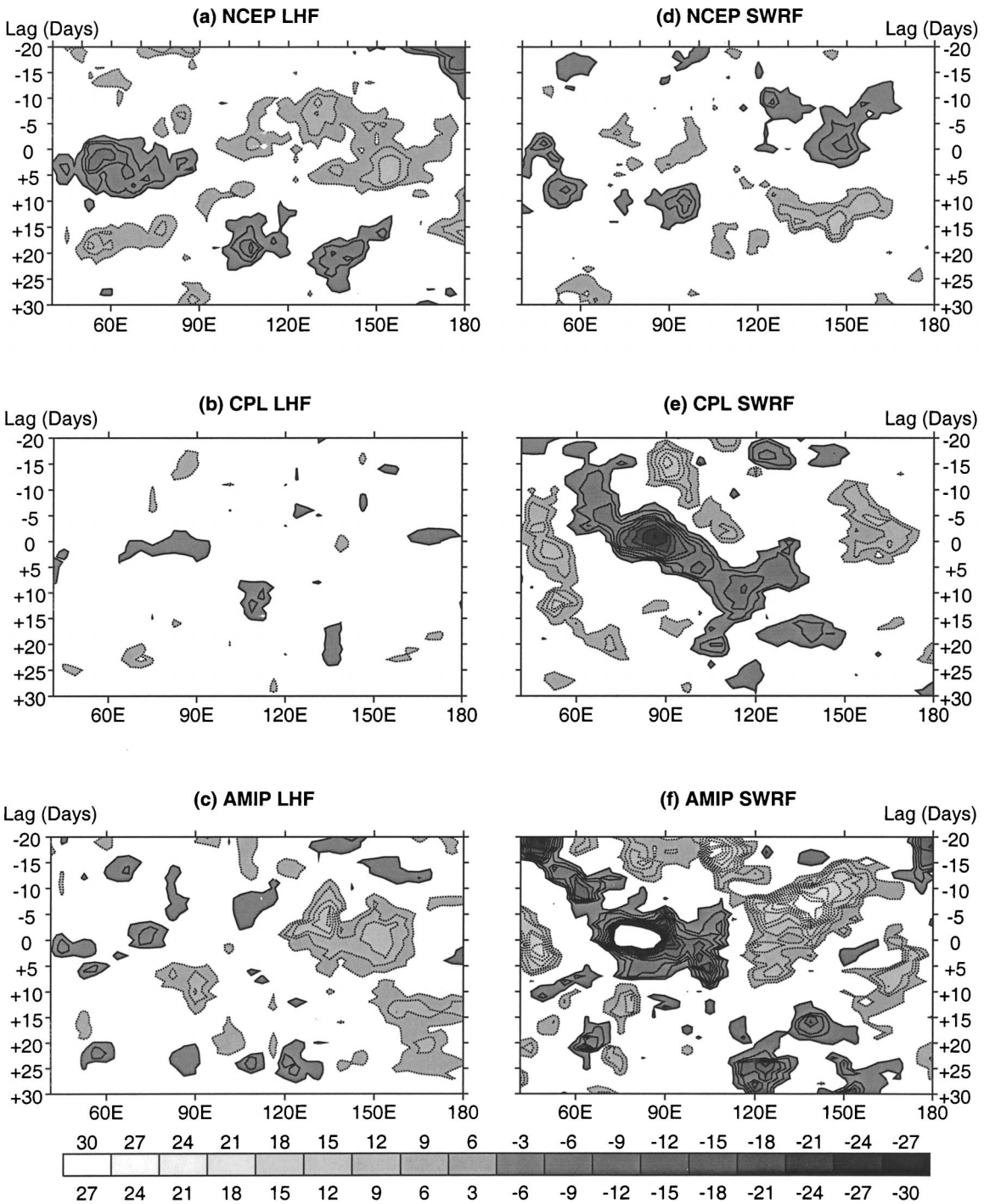


FIG. 9. Composite winter surface latent heat flux and shortwave heat flux anomaly Hovmoeller diagram for 10°N–10°S. Horizontal axis is longitude. Vertical axis is time (days) relative to day 0 of the composite. Only contours significant at the 90% level are shown. Shaded contours are surface fluxes (W $m^{-2}$). (a) NCEP reanalysis latent heat flux. (b) CPL latent heat flux. (c) AMIP latent heat flux. (d) NCEP reanalysis surface shortwave flux. (e) CPL surface shortwave flux. (e) AMIP surface shortwave flux.

anomaly concurrent with the convection, but misses the negative latent heat flux anomaly seen before the onset of convection in the observations (OBS). In the plot of SST and OLR, CPL shows a structure similar to the OBS with northward and southward-moving features, which are centered about the equator. For both the OBS and CPL, the low-level convergence structure is similar to the SST anomaly distribution, suggesting that the SST

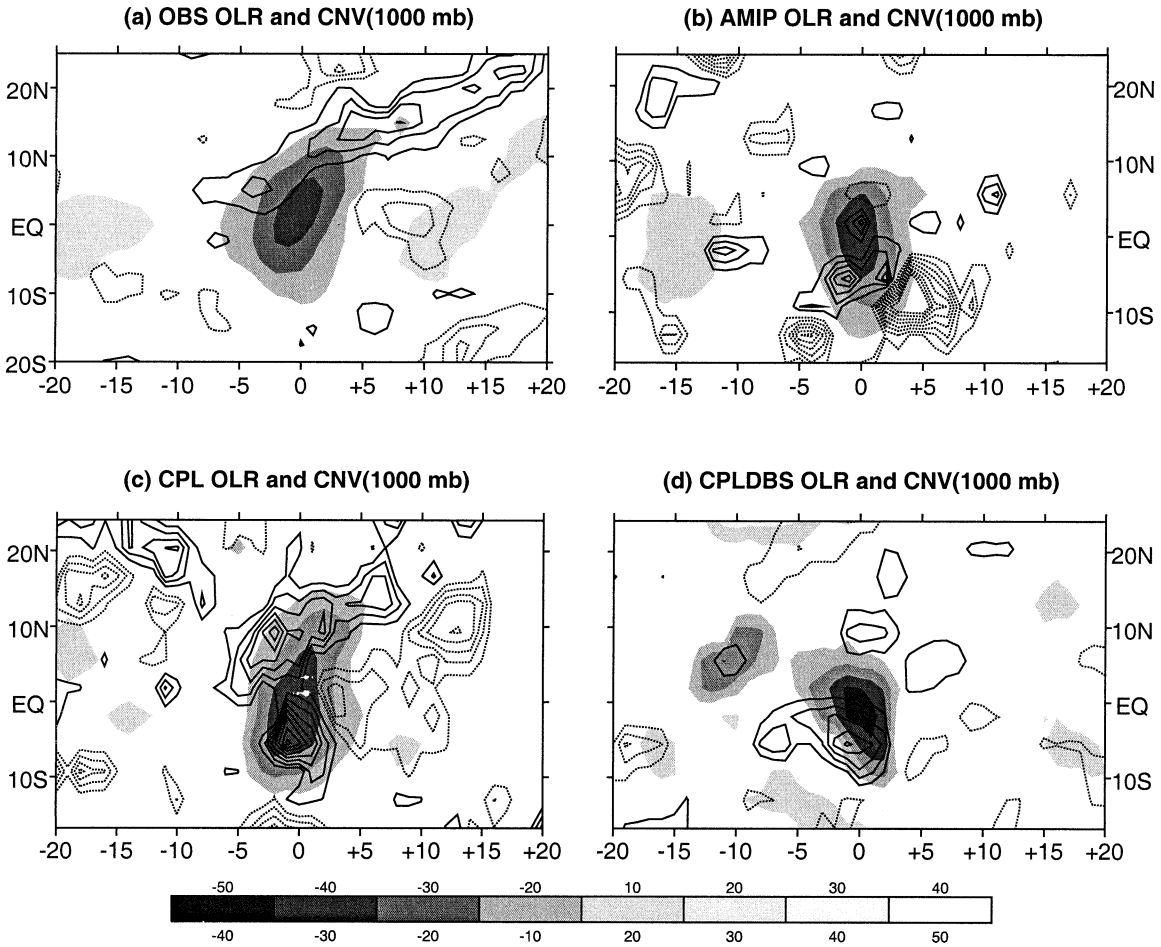


FIG. 10. Composite May–Jun OLR and 1000-mb convergence Hovmoeller diagram for 65°–95°E. Vertical axis is latitude. Horizontal axis is time (days) relative to day 0 of the composite. Only contours significant at the 90% level are shown. Shaded contours are OLR (W $m^{-2}$, contour interval is 5). Solid (dashed) contours convergence (divergence). Contour interval is 2.5 $\times$ $10^{-7}$ $s^{-1}$ and first contour is at 2.5 $\times$ $10^{-7}$ $s^{-1}$. (a) Observed OLR and 1000-mb convergence. (b) AMIP OLR and 1000-mb convergence. (c) CPL OLR and 1000-mb convergence. (d) CPLDBS OLR and 1000-mb convergence.

anomaly plays a role in determining the low-level convergence. CPL shows a clear link between the surface shortwave radiation and the convergence and SST anomalies (not shown), with the positive shortwave anomaly leading the low-level convergence, which, in turn, leads the convection. This phase relationship is not only evidence of air–sea coupling, but also reflects an essential characteristic of the coupled instability on the intraseasonal timescale. The unstable equatorial mode found in the coupled atmosphere–ocean system (Wang and Xie 1998) has precisely the same phase relationship as is seen here.

The CPL SST anomaly is well correlated with the low-level convergence, suggesting that here, as in Waliser et al. (1999), the SST anomaly helps organize the low-level convergence and strengthens the ISO, making northward propagation more pronounced in MJ. Note that the easterlies north of the convection are flowing into the region of warm SST anomaly in both the OBS and in CPL. This means that the CPL case has a stronger gradient across the convective anomaly with stronger convergence ahead and stronger divergence behind the equatorial OLR anomaly than is seen in AMIP.

In AMIP, the wind anomalies are centered about the equator, as is the latent heat flux anomaly. The northward-propagating mode is very strongly selected in the OBS, but less so in CPL and even less so in AMIP. The signal in the low-level convergence is quite weak, but what little there is associated with the eastward-moving equatorial mode. The wind and latent heat flux anomalies in CPLDBS are similar to those of AMIP and are omitted.

The MJ ISO northward propagation has been attributed to Rossby wave emission by equatorial convection (Kemball-Cook and Wang 2001; AS01; Lawrence and Webster 2001). Of the three runs, only CPL shows marked northward propagation over the Indian Ocean. CPL and CPLDBS share the same basic state, so that the likelihood of Rossby wave emission from equatorial convection should be equal in both cases; the difference

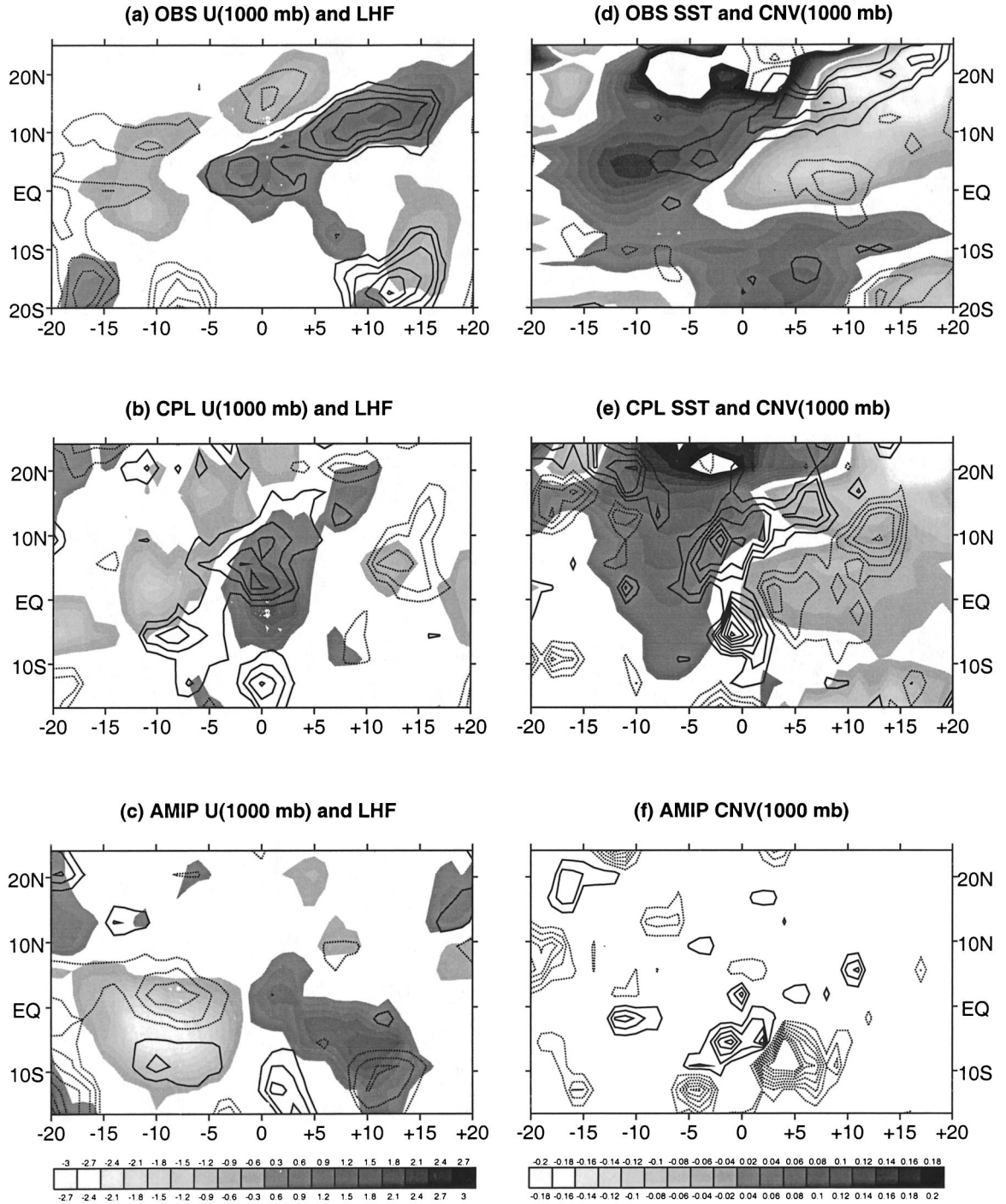


FIG. 11. Composite May–Jun SST, latent heat flux, and 1000-mb zonal wind Hovmoeller diagram for 65°–95°E. Vertical axis is latitude. Horizontal axis is time (days) relative to day 0 of the composite. Only contours significant at the 90% level are shown. Shaded contours for (a)–(c) are 1000-mb zonal wind. Contour interval is 0.3 m $s^{-1}$. Shaded contours (d)–(f) are SST. Contour interval is 0.6 K. (a)–(c) Solid (dashed) contours positive (negative) latent heat flux anomaly. Contour interval is 5 W $m^{-2}$ and first contour is at 5 W $m^{-2}$. (d)–(f) Solid (dashed) contours convergence (divergence). Contour interval is $2.5 \times 10^{-7}$ $s^{-1}$ and first contour is at $2.5 \times 10^{-7}$ $s^{-1}$. (a) NCEP reanalysis latent heat flux and 1000-mb zonal wind anomalies. (b) CPL latent heat flux and 1000-mb zonal wind anomalies. (c) AMIP latent heat flux and 1000-mb zonal wind anomalies. (d) NCEP reanalysis SST and convergence anomalies. (e) CPL SST and convergence anomalies. (f) AMIP convergence anomaly.

in the two MJ ISOs can be attributed to coupling. The similarity of the AMIP and CPLDBS runs suggests that the coupling is helping to destabilize the northward-moving mode by enhancing low-level convergence into the positive SST anomaly. In AMIP and CPLDBS, which lack the strengthening of the northward-moving lobe through air–sea interaction, only the eastward-moving mode is favored. The enhanced northward propagation in CPL is consistent with the improvement in the mean MJ heat source in CPL (Fig. 3).

## 6. Northwestward propagation in the western Pacific in August–October

The AO ISO is marked by prominent northwestward propagation of convection and circulation anomalies in the western Pacific. The observed AO ISO (Fig. 12a) shows coherent northward propagation of the convection, accompanied by a convergence anomaly that appears on the equator and tracks northward slightly ahead of the convection. Convection forms first along the equator in the western Pacific and then moves northward as an asymmetric Rossby wave is emitted by the equatorial convection (Kemball-Cook and Wang 2001). The AMIP case (Fig. 12b) shows a reasonable simulation of the northward propagation, with a low-level convergence anomaly propagating northward along with the OLR and leading it slightly. As in Fig. 12a, the southern lobe of the Rossby wave is present, though weaker than the northern lobe. In CPL and CPLDBS (Figs. 12c and 12d), however, no poleward propagation is visible in the OLR or in the low-level convergence.

To determine why northward propagation of ISO anomalies in the western Pacific is absent in AO in CPL and CPLDBS, we examine the coupled model basic state. Wang and Xie (1996) and Xie and Wang (1996) showed that the emission of Rossby waves by equatorial convection is favored in the presence of easterly vertical shear of the basic-state zonal wind. Figure 13 shows the August–October mean vertical shear of the zonal wind [defined as $U(200\text{ mb}) - U(850\text{ mb})$] and the composite OLR anomaly on the day on which convection reaches its maximum intensity in the equatorial western Pacific (day 0 of the composite).

In Fig. 13a, the equatorial convection has reached its maximum intensity and lies almost entirely within the region of easterly zonal wind shear. The basic state, then, is favorable for emission of a Rossby wave, whose northern lobe is more intense than the southern lobe because of the asymmetry about the equator in both the mean wind shear and sea surface temperatures (Kemball-Cook and Wang 2001). In CPL (and CPLDBS), the region of easterly vertical wind shear lies to the north of the equatorial convection, so that the convection is almost entirely within a region of westerly shear. Rossby wave emission is not favored, and the equatorial convection subsequently dissipates without significant northward or eastward propagation. The eastward propagation is limited because of the cold bias in the SSTs in the equatorial western Pacific in CPL.

The AMIP case is closer to the observations than is CPL. The region of maximum equatorial convection lies mostly within the region of easterly vertical shear, (Fig. 13c) and so an asymmetric Rossby wave resembling observations is emitted.

## 7. Discussion

A comparison of the ISO produced in coupled and uncoupled versions of the ECHAM-4 GCM shows that the uncoupled AMIP simulation does produce an intraseasonal oscillation. Therefore, our results suggest that the ISO is primarily a mode of the atmosphere, and that the ISO does not rely upon coupling between the ocean and atmosphere for its existence. However, interaction with the sea surface, while not critical for the existence of the ISO, plays a role in its organization and intensification, and also in the setting of its phase speed.

The most significant result of this study is that, during most of the year, the coupled run does produce an ISO that is improved, in spite of the fact that the basic state reached by the AGCM and ocean model together is less conducive to convection than is the model's AMIP run climatology. This suggests that coupling does play an intensifying role in the ISO, and may be part of the explanation for why AGCMs have had so much difficulty in simulating the tropical intraseasonal variability (Slingo et al. 1996).

The comparison of the CPL and AMIP composite winter ISO gives results closer to those of Waliser et al. (1999) than to those of Hendon (2000). As in Waliser et al. (1999), the addition of an interactive sea surface improved the low-level wind structure and increased the intensity, organization, and frequency of occurrence of the MJO. Also, similar to the results of Waliser et al. (1999), the ECHAM-4 model showed some intraseasonal modulation of the surface fluxes. The differences seen in the present study from the study of Hendon (2000), in which the model failed to produce any coherent surface fluxes, may be because the ECHAM-4 model basic state reproduces (albeit weakly) the observed low-level westerly winds in the Tropics, while the version of the GFDL model used in Hendon (2000) does not.

The ISO simulated by the model in both AMIP and CPL runs operates differently from the reanalysis ISO in that the shortwave radiation anomalies are twice as strong as the latent heat flux anomalies; in the reanalysis, these fluxes are of similar magnitudes. The large model shortwave radiation anomalies compensate for the small latent heat flux anomalies. The SST anomalies in CPL are tightly tied to the shortwave radiation anomalies, and the convergence anomalies are well correlated with the SST anomalies. The low-level convergence is also twice as strong in the model as in the reanalysis. In the model runs, the latent heat flux contribution to the build-

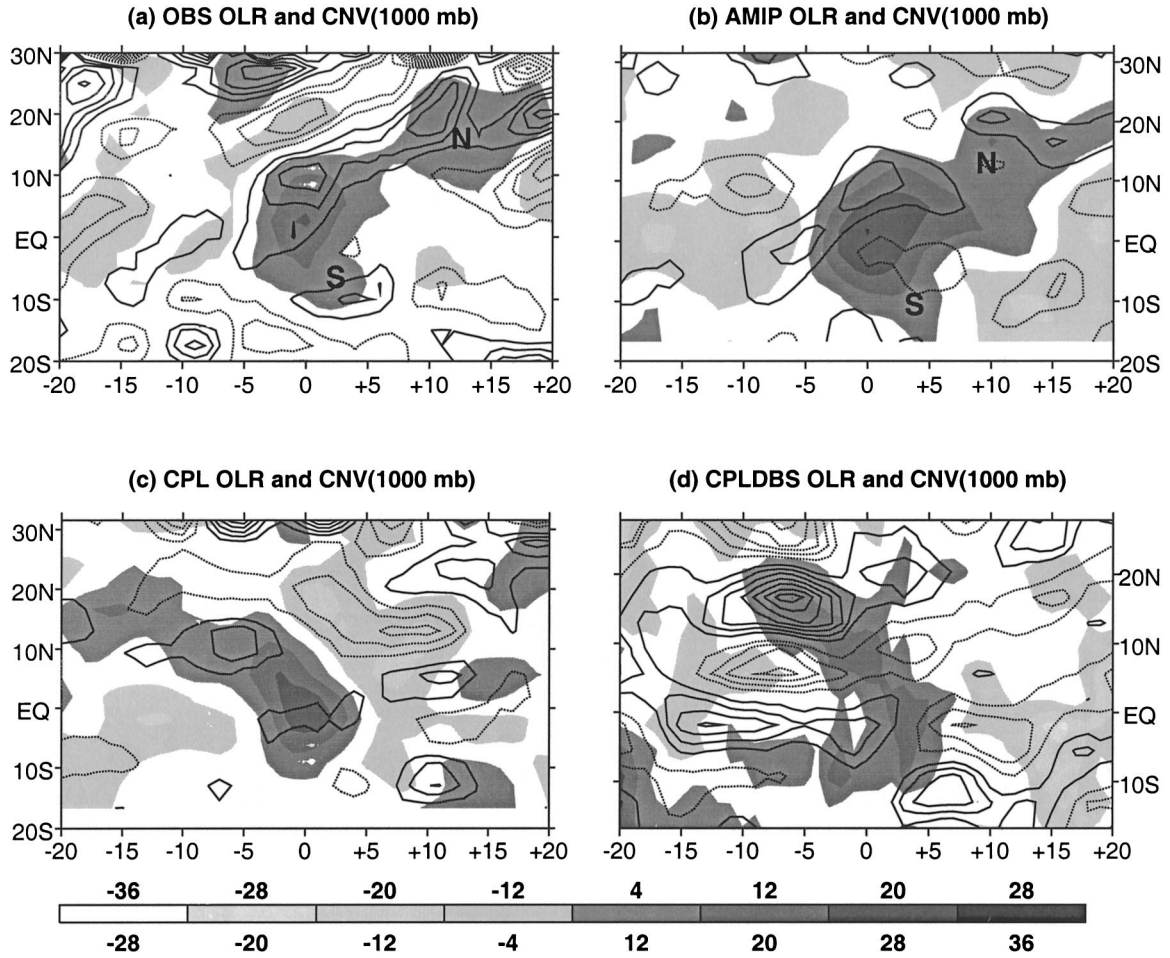


FIG. 12. Composite Aug–Oct OLR and 1000-mb convergence Hovmoeller diagram for 125°–170°E. Vertical axis is latitude. Horizontal axis is time (days) relative to day 0 of the composite. Only contours significant at the 90% level are shown. Shaded contours are OLR (W $m^{-2}$, contour interval is 5). Solid (dashed) contours convergence (divergence). Contour interval is 2.5 $\times$ $10^{-7}$ $s^{-1}$ and first contour is at 2.5 $\times$ $10^{-7}$ $s^{-1}$. Northern (southern) lobe of the Rossby wave is indicated by the letter N (S) where identifiable. (a) Observed OLR and 1000-mb convergence. (b) AMIP OLR and 1000-mb convergence. (c) CPL OLR and 1000-mb convergence. (d) CPLDBS OLR and 1000-mb convergence.

up of moisture to the east of the convection is negligible compared to the contribution of convergence. So it appears that the model is compensating for the small latent heat flux and may be generating a reasonable ISO for the wrong reasons. Waliser et al. (1999) also found that low-level convergence (mostly due to the meridional wind) was instrumental in the moisture buildup. This result is similar to our findings here.

The results of this experiment show that for winter and MJ, coupling the atmosphere to an ocean model produces a better ISO by enhancing convergence into the region occupied by the positive SST anomaly. In MJ, the presence of this mechanism destabilizes the northward-propagating mode of the ISO in the Indian Ocean in CPL, although it is still weaker than observed. This is a significant improvement over the AMIP run, in which there was no northward propagation of convection in MJ.

The ECHAM-4 model in both coupled and uncoupled configuration is better able to simulate the intraseasonal variability in winter than in summer. This is most likely because the model basic state in AMIP and CPL is closest to the observed basic state in winter. In winter, both model runs capture the large-scale features of the diabatic heating distribution and the zonal winds. In summer, when the model runs miss some salient features of the observed basic state, the ISO simulation is less accurate.

The August–October results also point out the importance of the basic state for the mode selection. The CPL/CPLDBS basic state does not allow the existence of the northwestward-moving mode, because the vertical wind shear in the equatorial western Pacific has the wrong sign. In a situation where the modeled basic state is incorrect, coupling does not necessarily improve the quality of the simulation, consistent with the result of Hendon (2000).

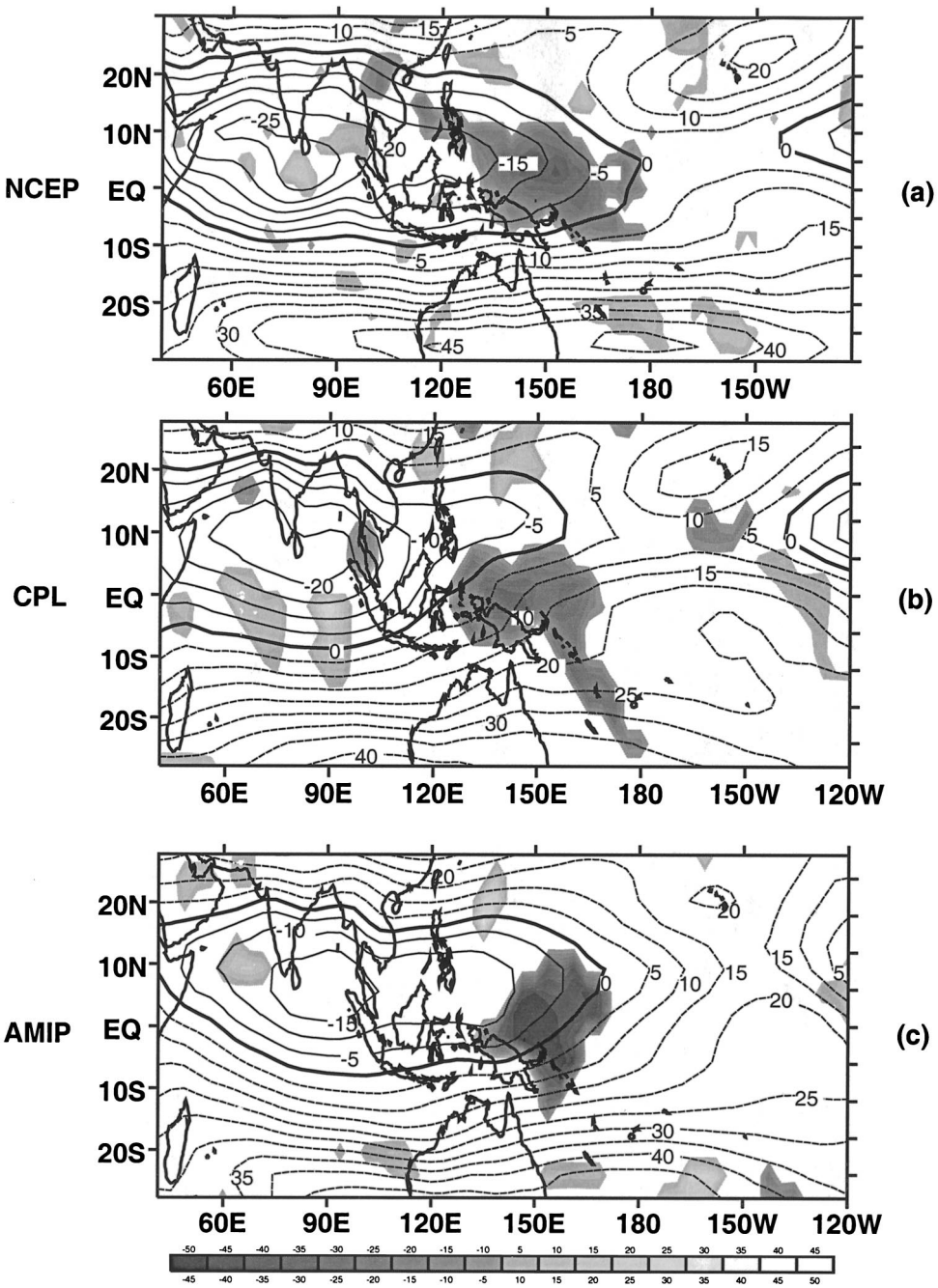


FIG. 13. Composite Aug–Oct OLR for day 0 and Aug–Oct mean vertical shear of the zonal wind. For all three panels, shaded contours are OLR anomaly. Contour interval is 5 W $m^{-2}$ and first contour is at 5 W $m^{-2}$. Only contours significant at the 90% level are shown. (a) NCEP vertical shear and observed day 0 OLR. (b) CPL vertical shear and day 0 OLR. (c) AMIP vertical shear and day 0 OLR.

The lack of the correct basic state in AO means that it is not possible to know whether coupling would be helpful in the simulation of the ISO in this region. The fact that the AMIP simulation looks so reasonable suggests that the presence of the right basic state is at least as important as air–sea interaction. However, there is substantial air–sea interaction in this region, as noted by Kemball-Cook and Wang (2001), and a worthwhile extension of this study will be to examine the AO ISO with a GCM that correctly simulates the mean shear. Kemball-Cook and Wang (2002, manuscript submitted to *J. Atmos. Sci.*), have shown with a simple coupled model in which the atmosphere's basic state can be easily controlled that it is possible to generate the north-

westward-moving AO mode only when the basic-state vertical wind shear has the correct sign. In this simplified model, the sign of the basic state vertical wind shear is more important than air–sea interaction in generating this mode, as is suggested by the CPL and CPLDBS runs in the present study.

*Acknowledgments.* We thank Dr. Harry Hendon for providing the computer program for generating space–time spectra. Comments by Dr. Duane Waliser and two anonymous reviewers significantly improved an earlier version of this manuscript. NCEP–NCAR reanalysis data were provided by the NOAA–CIRES Climate Diagnostics Center, Boulder, Colorado, from their Website at www.cdc.noaa.gov. This research was supported by the Climate Dynamics Program, National Science Foundation under Grants ATM 96-13776 and ATM00-73023. The International Pacific Research Center is sponsored in part by the Frontier Research System for Global Change.

## REFERENCES

Annamalai, H., and J. M. Slingo, 2001: Active/break cycles: Diagnosis of the intraseasonal variability of the Asian summer monsoon. *Climate Dyn.,* **18,** 85–102.

Chen, T.-C., and M. Murakami, 1988: The 30–50 day variation of convective activity over the western Pacific region with the emphasis on the northwestern region. *Mon. Wea. Rev.,* **116,** 892–906.

Emanuel, K. A., 1987: An air–sea interaction model of the intraseasonal oscillations in the Tropics. *J. Atmos. Sci.,* **44,** 2324–2340.

Flatau, M., P. J. Flatau, P. Phoebus, and P. Niiler, 1997: The feedback between equatorial convection and local radiative and evaporative processes: The implications for intraseasonal oscillations. *J. Atmos. Sci.,* **54,** 2373–2386.

Fu, X., and B. Wang, 2001: A coupled modeling study of the seasonal cycle of Pacific cold tongue. Part I: Simulation and sensitivity experiments. *J. Climate,* **14,** 765–779.

Gates, W. L., 1992: AMIP: The Atmospheric Model Intercomparison Project. *Bull. Amer. Meteor. Soc.,* **73,** 1962–1970.

Graham, N., and T. P. Barnett, 1987: Observations of sea surface temperature and convection over tropical oceans. *Science,* **238,** 657–659.

Gutzler, D. S., G. N. Kiladis, G. A. Meehl, K. M. Weickmann, and M. Wheeler, 1994: The global climate of December 1992–February 1993. Part II: Large-scale variability across the tropical western Pacific during TOGA COARE. *J. Climate,* **7,** 1606–1622.

Hartmann, D. L., and M. Michaelson, 1989: Intraseasonal periodicities in Indian rainfall. *J. Atmos. Sci.,* **46,** 2838–2862.

——, ——, and S. Klein, 1992: Seasonal variations of tropical intraseasonal oscillations: A 20–25 day oscillation in the western Pacific. *J. Atmos. Sci.,* **49,** 1277–1289.

Hayashi, Y., 1982: Space–time spectral analysis and its application to atmospheric waves. *J. Meteor. Soc. Japan,* **60,** 156–171.

Hendon, H., 2000: Impact of air–sea coupling on the Madden–Julian oscillation in a general circulation model. *J. Atmos. Sci.,* **57,** 3939–3952.

——, and M. L. Salby, 1994: The life cycle of the Madden–Julian oscillation. *J. Atmos. Sci.,* **51,** 2207–2219.

——, and J. Glick, 1997: Intraseasonal air–sea interaction in the tropical Indian and Pacific Oceans. *J. Climate,* **10,** 647–661.

——, D. Waliser, and C. Gautier, 1998: The influence of the Madden–Julian oscillation on ocean surface heat fluxes and sea surface temperature. *J. Climate,* **11,** 1057–1072.

Kalnay, E., and Coauthors, 1996: The NCEP/NCAR 40-Year Reanalysis Project. *Bull. Amer. Meteor. Soc.,* **77,** 437–471.

Kemball-Cook, S., and B. Wang, 2001: Equatorial waves and air–sea interaction in the boreal summer intraseasonal oscillation. *J. Climate,* **14,** 2923–2942.

Krishnamurti, T. N., and D. Subrahmanyam, 1982: The 30–50 day mode at 850 mb during MONEX. *J. Atmos. Sci.,* **39,** 2088–2095.

——, D. Dosterhof, and A. Mehta, 1988: Air–sea interaction on the time scale of 30–50 days. *J. Atmos. Sci.,* **45,** 1304–1322.

Lau, K.-M., and C.-H. Sui, 1997: Mechanisms of short-term sea surface temperature regulation: Observations during TOGA COARE. *J. Climate,* **10,** 465–472.

Lawrence, D. M., and P. J. Webster, 2001: Interannual variations of the intraseasonal oscillation in the south Asian summer monsoon region. *J. Climate,* **14,** 2910–2922.

Liebmann, B., and C. Smith, 1996: Description of a complete (interpolated) OLR dataset. *Bull. Amer. Meteor. Soc.,* **77,** 1275–1277.

Madden, R. A., and P. R. Julian, 1972: Description of global-scale circulation cells in the tropics with a 40–50 day period. *J. Atmos. Sci.,* **29,** 1109–1123.

——, and ——, 1994: Observations of the 40–50-day tropical oscillation—A review. *Mon. Wea. Rev.,* **122,** 814–837.

Maloney, E., and D. Hartmann, 1998: Frictional moisture convergence in a composite life cycle of the Madden–Julian oscillation. *J. Climate,* **11,** 2387–2403.

Murakami, T., T. Nakazawa, and J. He, 1984: On the 40–50 day oscillations during the 1979 Northern Hemisphere summer. I: Phase propagation. *J. Meteor. Soc. Japan,* **62,** 440–468.

Neelin, J. D., I. M. Held, and K. H. Cook, 1987: Evaporation–wind feedback and low-frequency variability in the tropical atmosphere. *J. Atmos. Sci.,* **44,** 2341–2348.

Niiler, P. P., and E. B. Kraus, 1977: One-dimensional models of the upper ocean. *Modeling and Prediction of the Upper Layers of the Ocean,* E. B. Kraus, Ed., Pergamon Press, 143–172.

Nitta, T., 1987: Convective activities in the tropical western Pacific and their impacts on the Northern Hemisphere summer circulation. *J. Meteor. Soc. Japan,* **65,** 165–171.

Press, W. H., S. A. Teukolsky, W. T. Vetterling, and B. P. Flannery, 1986: *Numerical Recipes.* Cambridge University Press, 848 pp.

Roeckner, E., and Coauthors, 1996: The atmospheric general circulation model ECHAM-4: Model description and simulation of present-day climate. Max-Planck-Institut für Meteorologie, Rep. 218, 90 pp.

Rui, H., and B. Wang, 1990: Development characteristics and dynamic structure of tropical intraseasonal convection anomalies. *J. Atmos. Sci.,* **47,** 357–379.

Seager, R., S. E. Zebiak, and M. A. Cane, 1988: A model of tropical Pacific sea surface temperature climatology. *J. Geophys. Res.,* **93** (C2), 1265–1280.

Shinoda, T., H. Hendon, and J. Glick, 1998: Intraseasonal variability of surface fluxes and sea surface temperature in the tropical western Pacific and Indian Oceans. *J. Climate,* **11,** 1685–1702.

——, ——, and ——, 1999: Intraseasonal surface fluxes in the tropical western Pacific and Indian Oceans from NCEP reanalyses. *Mon. Wea. Rev.,* **127,** 678–693.

Slingo, J. M., and Coauthors, 1996: The intraseasonal oscillation in 15 atmospheric general circulation models: Results from an AMIP diagnostic subproject. *Climate Dyn.,* **12,** 325–357.

Sundqvist, H., 1978: A parameterization scheme for non-convective condensation including prediction of cloud water content. *Quart. J. Roy. Meteor. Soc.,* **104,** 677–690.

Tiedtke, M., 1989: A comprehensive mass flux scheme for cumulus parameterization in large-scale models. *Mon. Wea. Rev.,* **117,** 1779–1800.

Waliser, D. E., K.-M. Lau, and J.-H. Kim, 1999: The influence of coupled sea surface temperatures on the Madden–Julian oscil-

lation: A model perturbation experiment. *J. Atmos. Sci.,* **56,** 333–358.
Wang, B., 1988: Dynamics of tropical low-frequency waves: An analysis of the moist Kelvin wave. *J. Atmos. Sci.,* **45,** 2051–2065.
——, and H. Rui, 1990: Synoptic climatology of transient tropical intraseasonal convection anomalies: 1975–1985. *Meteor. Atmos. Phys.,* **44,** 43–61.
——, and T. Li, 1994: Convective interaction with boundary-layer dynamics in the development of a tropical intraseasonal system. *J. Atmos. Sci.,* **51,** 1386–1400.
——, and X. Xie, 1996: Low frequency equatorial waves in a sheared zonal flow. Part I: Stable waves. *J. Atmos. Sci.,* **53,** 449–467.
——, and ——, 1998: Coupled modes of the warm pool climate system: Part I: The role of air–sea interaction in maintaining the Madden–Julian oscillation. *J. Climate,* **11,** 2116–2135.
——, T. Li, and P. Chang, 1995: An intermediate model of the tropical ocean. *J. Phys. Oceanogr.,* **25,** 1599–1616.
Weller, R. A., and S. P. Anderson, 1996: Surface meteorology and air–sea fluxes in the western equatorial Pacific warm pool during the TOGA Coupled Ocean–Atmosphere Response Experiment. *J. Climate,* **9,** 1959–1990.
Woolnough, S. J., J. M. Slingo, and B. J. Hoskins, 2000: The relationship between convection and sea surface temperature on intraseasonal timescales. *J. Climate,* **13,** 2086–2104.
Xie, X., and B. Wang, 1996: Low frequency equatorial waves in a sheared zonal flow. Part II: Unstable waves. *J. Atmos. Sci.,* **53,** 3589–3605.
Yasunari, T., 1979: Cloudiness fluctuations associated with the Northern Hemisphere summer monsoon. *J. Meteor. Soc. Japan,* **57,** 227–242.
Zhang, C., 1996: Atmospheric intraseasonal variability at the surface in the tropical western Pacific Ocean. *J. Atmos. Sci.,* **53,** 739–758.
——, and ——, 2000: Intraseasonal surface cooling in the equatorial Pacific. *J. Climate,* **13,** 2261–2276.
Zhu, B., and B. Wang, 1993: The 30–60-day convection seesaw between the tropical Indian and western Pacific Oceans. *J. Atmos. Sci.,* **50,** 184–199.